

Localized surface electromagnetic waves in CrI₃-based magnetophotonic structures

Anastasiia A. Pervishko,^{1,2} Dmitry Yudin,^{3,1} Vijay Kumar Gudelli,⁴ Anna Delin,^{1,5} Olle Eriksson,^{1,6} and Guang-Yu Guo^{7,4}

¹*Department of Physics and Astronomy, Materials Theory Division, Uppsala University, Box 516, SE-75120 Uppsala, Sweden*

²*ITMO University, Saint Petersburg 197101, Russia*

³*Skolkovo Institute of Science and Technology, Moscow 121205, Russia*

⁴*Physics Division, National Center for Theoretical Sciences, Hsinchu 30013, Taiwan*

⁵*Department of Applied Physics, School of Engineering Sciences,*

KTH Royal Institute of Technology, Electrum 229, SE-16440 Kista, Sweden

⁶*School of Science and Technology, Örebro University, SE-70182 Örebro, Sweden*

⁷*Department of Physics and Center for Theoretical Physics, National Taiwan University, Taipei 10617, Taiwan*

(Dated: June 13, 2022)

Resulting from strong magnetic anisotropy two-dimensional ferromagnetism was recently shown to be stabilized in chromium triiodide, CrI₃, in the monolayer limit. While its properties remain largely unexplored, it provides a unique material-specific platform to unveil electromagnetic properties associated with coupling of modes. Indeed, trigonal symmetry in the presence of out-of-plane magnetization results in a non-trivial structure of the conductivity tensor, including the off-diagonal terms. In this paper, based on the results of *ab initio* calculations of the conductivity tensor, we study the surface electromagnetic waves localized in a CrI₃-based structure. In particular, we provide an estimate for the critical angle corresponding to the surface plasmon polariton generation in the Kretschmann-Raether configuration by a detailed investigation of reflectance spectrum and magnetic field distribution for different CrI₃ layer thicknesses. We also study the bilayer structure formed by two CrI₃ layers separated by a SiO₂ spacer and show that the surface plasmon resonance can be obtained at the outer interface of the proposed system depending on the spacer thickness.

Introduction. Studies of two-dimensional materials has been booming since the successful exfoliation of the monolayer graphene structure [1]. This pioneering work initiated the search for alternative two-dimensional structures of hexagonal lattices with similar electronic, optical, and transport properties for the potential utility of faster information processing. Lately, the experimental activity has resulted in the discovery of other members of this family, including monolayers of transition metal dichalcogenides [2], phosphorene [3, 4], silicene [5–7], germanene [8] and stanene [9] to name a few. Targeted data-mining efforts have also been devoted to the identification of novel two-dimensional materials [10–12], and in fact some of these theoretical predictions have been verified experimentally [13–15].

Of particular importance for the present investigation, is the recent discovery of intrinsic ferromagnetism in Cr₂Ge₂Te₆ and CrI₃-based van der Waals structures, where magnetism was studied on monolayers using magneto-optical Kerr effect [15, 16]. Such investigations open avenues for the direct applications of this class of materials, for ultrathin magnetic sensors and spin filters of high efficiency [17–22]. For a long time magnetism was not believed to be present in low dimensional magnetic structures, owing to the Mermin-Wagner theorem [23], which in the isotropic Heisenberg model forbids the formation of collinear magnetic ordering in one- and two-dimensional systems, at any finite temperature. Nevertheless, in CrI₃ crystals magnetic ordering is observed experimentally, and is demonstrated to be stabilized by the

large out-of-plane magnetic anisotropy that relaxes the Mermin-Wagner constraint. The magnetic anisotropy turns out to substantially suppress transverse spin fluctuations resulting in ferromagnetic ordering being clearly detectable at finite temperatures, even in monolayer systems.

Experimental findings on CrI₃-based monolayers, including magnetic exchange coupling and magnetic anisotropy, are supported by the results of first-principles calculations [24–26]. The magnetic properties of this system are governed by the Cr³⁺ ions, which are arranged in a two dimensional hexagonal Bravais lattice, while the non-magnetic I[−] ions form an octahedral coordination around Cr. The combination of both relativistic spin-orbit coupling of the heavier ligand I atoms, as well as single-ion anisotropy of Cr atoms, leads to the strong magnetic anisotropy of the structure [24, 25, 27–29]. Unfortunately, much less is known regarding electromagnetic properties of chromium triiodide monolayers. To remedy some of this shortcoming, we explore here a monolayer of chromium triiodide, from the perspective of electromagnetic theory with the focus on plasmon excitations. The appearance and propagation of surface electromagnetic waves at the interface between two media has been extensively studied over last decades [30–32]. Initiated by the description of surface waves at the boundary between the metal and dielectric material, their presence has also been confirmed on specific semiconductor/dielectric interfaces, including a whole family of two-dimensional materials [33–38]. In this paper,

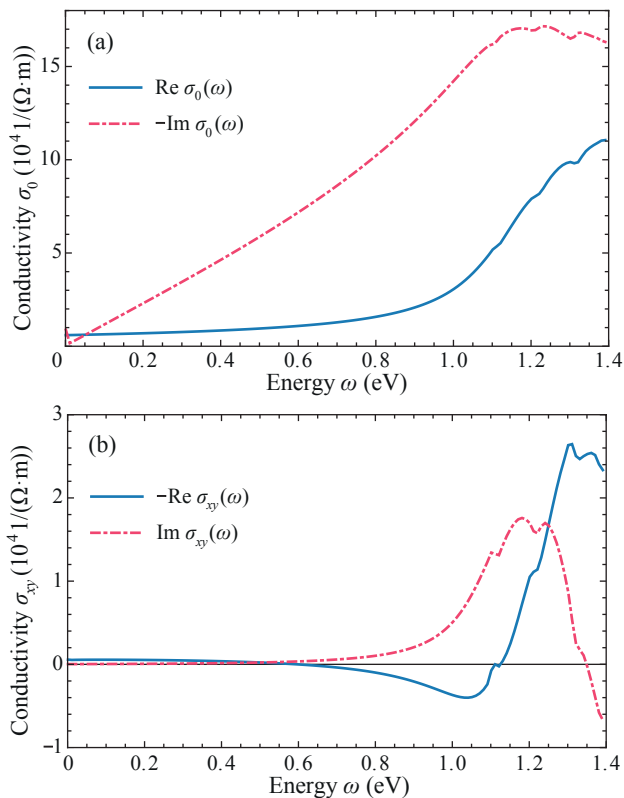


FIG. 1. In-plane (a) diagonal $\sigma_0(\omega)$ and (b) off-diagonal $\sigma_{xy}(\omega)$ components of the conductivity tensor as obtained from the Kubo formula combined with the results of first principles calculations within GGA+ U approximation [39].

we base our considerations on the solution of a set of Maxwell's equation on condition of the microscopic nature of the conductivity tensor obtained from *ab initio* calculations. We address several systems containing CrI_3 layers, in order to study the possibility of surface electromagnetic wave generation in this class of materials.

Conductivity of a monolayer chromium triiodide. For the calculation of the conductivity tensor of the CrI_3 -monolayer we applied density functional theory, with the use of the accurate, fully relativistic projector augmented wave (PAW) method, as implemented in the Vienna *ab initio* simulation package (VASP) [40, 41]. This allows us to include the effect of spin-orbit interaction, which is important for details of the electronic structure as well as for the off-diagonal elements of the conductivity tensor. Exchange-correlation potential in form of the Perdew-Burke-Ernzerhof parametrization [42] was applied within the generalized gradient approximation (GGA), with the account of on-site Coulomb repulsion among Cr $3d$ electrons (GGA+ U) [43, 44]. Similar to a previous study on $\text{Cr}_2\text{Ge}_2\text{Te}_6$ [28], we adopt $U = 1$ eV. We also scanned U through a range between 0 and 3 eV, thus allowing to investigate the influence of U on the optical properties. From these calculations, a material-specific conductivity tensor can be worked out based on the Kubo

formula [45]. A proper account of trigonal symmetry of a honeycomb lattice suggests only three components to be independent, namely $\sigma_0(\omega) \equiv \sigma_{xx}(\omega) = \sigma_{yy}(\omega)$, $\sigma_{yx}(\omega) = -\sigma_{xy}(\omega)$, and $\sigma_{zz}(\omega)$ with the rest being zero. The results of the GGA+ U calculations [39] for in-plane components of the conductivity tensor, $\sigma_0(\omega)$ and $\sigma_{xy}(\omega)$, are shown in Fig. 1. It should be emphasized that the conductivity of a monolayer of CrI_3 does not differ qualitatively from the behavior of bulk, as reported in Ref. [39], and therefore the results presented in Fig. 1 can be generalized to situations involving thicker CrI_3 layers.

A close inspection of Fig. 1 clearly reveals that for energies $\omega \lesssim 1.2$ eV the transverse component of the conductivity tensor $\sigma_{xy}(\omega)$ is one-two orders of magnitude smaller than the longitudinal one. In addition to that, it is interesting to note that for small energies, the imaginary part of the diagonal component of the conductivity tensor is negative while the real part is small. These are conditions that might give rise to the surface plasmon wave generation in CrI_3 layer, and this possibility will be discussed below.

Dispersion of surface electromagnetic waves. Generation, propagation and detection of plasmon excitations, resulting from the coupling between electromagnetic field and charge density waves of a conducting media, are of central importance of the rapidly advancing area of plasmonics [31]. In this context, chromium triiodide with its unique magneto-optical properties serves as a candidate for hosting surface electromagnetic waves formed in this monolayer structure. To outline the mechanism underlying the emergence and stability of surface plasmon polaritons in a CrI_3 monolayer, we inspect Maxwell's equations in the geometry shown schematically in Fig. 2a. The magnetic CrI_3 layer of thickness d is positioned at $z = 0$ with the \hat{z} axis pointing out from an insulating medium represented by a glass prism with constant permittivity ε_1 ($z < 0$). Outside the CrI_3 layer is air with permittivity $\varepsilon_2 = 1$. Without loss of generality, we suppose the electromagnetic wave to propagate along the \hat{x} axis with the propagation constant q and consider an evanescent solution which decays exponentially along the \hat{z} axis, $\propto e^{-\kappa|z|+iqx}$.

Being a highly conducting material, as shown in Figs. 1a-b, chromium triiodide monolayers lead to the discontinuity of the magnetic field at the boundary $z = 0$, $\hat{z} \times (\mathbf{H}_2 - \mathbf{H}_1) = \hat{\sigma}(\omega) \mathbf{E}^{\text{in}}$, while leaving the in-plane components of the electric field $\mathbf{E}^{\text{in}} = (E_x, E_y)$ unchanged, $\mathbf{E}_1^{\text{in}} = \mathbf{E}_2^{\text{in}}$. Thus, under these specified boundary conditions, one may obtain an expression for the dispersion [34–36, 46]:

$$\left(\frac{i\sigma_0}{\omega\varepsilon_0} + \frac{\varepsilon_1}{\kappa_1} + \frac{\varepsilon_2}{\kappa_2} \right) \left(\frac{i\sigma_0}{c\varepsilon_0} k_0 - \kappa_1 - \kappa_2 \right) = \left(\frac{\sigma_{xy}}{c\varepsilon_0} \right)^2, \quad (1)$$

where $k_0 = \omega/c$, while ε_0 and c denote the vacuum permittivity and speed of light respectively, and with $\kappa_{1,2}^2 = q^2 - \varepsilon_{1,2}k_0^2$ on either side of the monolayer. In

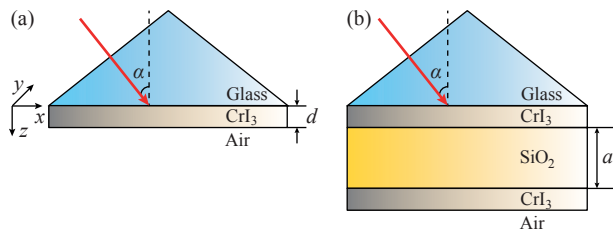


FIG. 2. The system under consideration: (a) the CrI_3 layer of thickness d is placed on top of a glass prism with permittivity ϵ_1 , while the air permittivity is ϵ_2 . The light is incident at the interface between glass and CrI_3 at the angle α ; (b) the bilayer structure is formed by two thin CrI_3 layers separated by a SiO_2 layer of thickness a , with refractive index n_{SiO_2} . Light is injected into the structure via a glass prism at the angle α .

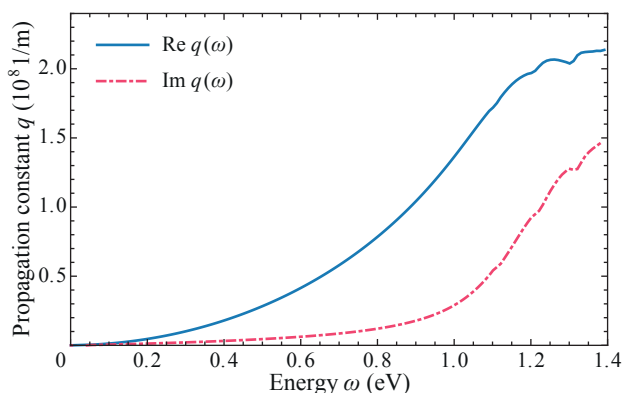


FIG. 3. The dispersion relation of surface electromagnetic waves $q(\omega)$ obtained as the solution to Eq. (1). It is clearly visible that in the energy window up to 1.2 eV the imaginary part of propagation constant is almost zero $\text{Im}q(\omega) \approx 0$, favoring the generation of surface plasmon polaritons along the CrI_3 boundary.

Eq. (1) the first multiplier on the left-hand side stands for the dispersion of a transverse electric (TE) mode, whereas the second one represents a transverse magnetic (TM) mode. Interestingly, the presence of the off-diagonal component, $\sigma_{xy}(\omega)$, on the right hand side of Eq. (1) results in the electromagnetic wave being of hybrid nature, with the mixing being proportional to $\sigma_{xy}(\omega)$ squared.

Numerical solution to Eq. (1) allows to identify the dispersion of localized surface electromagnetic waves, as shown in Fig. 3. The imaginary part, $\text{Im}q(\omega)$, defines the attenuation constant and is almost negligible in a relatively wide spectral region (up to $\omega \simeq 1.2$ eV), thus favoring the formation and propagation of surface plasmon polaritons bound to the ferromagnetic CrI_3 monolayer. However, the imaginary part of $\text{Im}q(\omega)$ becomes rather pronounced for higher frequencies, which takes place in the vicinity of interband transitions corresponding to the absorption edge. Noteworthy, the solution to Eq. (1) inherits the properties of TM plasmon with al-

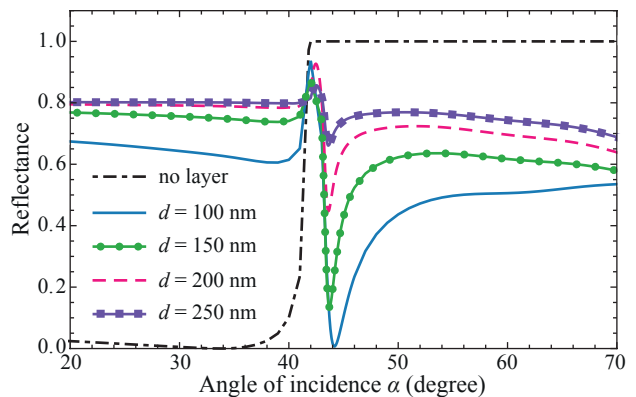


FIG. 4. Reflectance spectrum, characterizing the ratio of the reflected power to the input power (we put 1 W throughout the simulations) in the glass/ CrI_3 /air Kretschmann-Raether configuration (see Fig. 2a) given by the exact solution to Maxwell's equations with $\lambda = 1238$ nm for different CrI_3 layer thicknesses, d . For $d = 100$ nm the curve drops down to almost zero at $\alpha_0 = 44.1^\circ$ (blue solid line), which corresponds to the surface plasmon resonance while the total internal reflection of the incident electromagnetic field in the glass/air system without CrI_3 layer takes place at $\alpha = 41.8^\circ$ (black dot-dashed line). For $d > 100$ nm the maximum reflectance peak decreases and becomes narrower with the increase of the layer thickness. It almost vanishes at $d = 250$ nm (purple solid-squared line), while for $d < 100$ nm the surface plasmon resonance does not appear since there is not enough thickness to absorb the incident light.

most negligible impact from TE-mode (the absence of TE-mode is attributed to the lack of magnetic response in the system). Remarkably, upon inverting the plot in Fig. 3 we reproduce the well-known square-root behavior at small momenta, $\omega \propto \sqrt{q}$, with proportionality parameter $21.883 \text{ GHz} \cdot \text{m}^{-1/2}$. In what follows, we will explore the field distribution upon numerically solving Maxwell's equations.

Electromagnetic modeling. To prove the presence of surface electromagnetic waves bound by a magnetic monolayer, we simulate the propagation of TM-polarized electromagnetic field through a thin film of chromium triiodide in the Kretschmann-Raether (KR) configuration (Fig. 2a) [47–52]. This method is known to be quite ubiquitous in generating surface plasmon polaritons. The standard setup consists of a glass prism and a thin film of a lossy material. In our study the latter is the chromium triiodide layer, of thickness d , covered by an insulating medium that has a lower refractive index, compared to the glass prism on the opposite side of the chromium triiodide layer. For incident angles greater than the angle of the total internal reflection, the light reaching the boundary between the prism and the thin film material is converted to the evanescent wave at the other side of the boundary, thus ensuring the coupling to the surface electromagnetic waves. The maximum coupling occurs when the wave vector of the incident light matches the value of the surface plasmon propagation constant. In

the reflectance spectrum, the excitation of the surface plasmon polaritons manifests itself as a dip of the reflectance curve, taking place at higher angles compared to the peak representing the effect of total internal reflection (see Fig.4). The marked dip of the reflectance curve in Fig.4 stands for the effect of total absorption of the electromagnetic field energy, which is accompanied the in surface plasmon generation.

To study light propagation through the system described in Fig. 2a, we solve numerically a set of Maxwell's equations with account for electromagnetic boundary conditions at the surface. We consider a TM-polarized field, incident on the prism at the angle α , that is characterized by the following parameters: $|H_y| = 1$ A/m, the frequency is $f_0 = 242$ THz, and input power 1 W. This frequency has been chosen to make the effect as pronounced as possible in the simulations. The refractive indices on both sides of the chromium triiodide monolayer were taken to be: $n_1=1.5$ (for glass) and $n_2=1$ (for air). For this energy of the field, the components of the monolayer's conductivity tensor were calculated to be: $\sigma_0 = (0.307228 - 1.4240759i) \times 10^5 \Omega^{-1} \cdot \text{m}^{-1}$, $\sigma_{xy} = (0.508205 + 0.369802i) \times 10^4 \Omega^{-1} \cdot \text{m}^{-1}$ (see Fig. 1).

A close look at the results of numerical simulation of the reflectance spectrum for different CrI₃ film thicknesses shown in Fig. 4 reveal that the resonance angle of surface plasmon polaritons for glass/CrI₃/air KR configuration ranges from $\alpha = 43.6^\circ$ to 44.1° for d between 100 and 250 nm whereas the angle of total internal reflection for the system glass/air is $\alpha = 41.8^\circ$. Comparing the position of the surface plasmon dip, one can see that the thickness of the CrI₃ layer, d , is an important parameter for surface plasmon generation in the here investigated system. The optimal thickness, resulting in almost zero reflectance value (≈ 0.005 a.u.), equals $d = 100$ nm. This demonstrates a very efficient excitation of surface plasmons at these conditions, while for the thinner CrI₃ layers the surface plasmon resonance is less pronounced because there is not enough thickness to absorb light and excite plasmons. Subsequent variation of the CrI₃ layer thickness ($d > 100$ nm) results in a narrowing and a decrease of the resonance peak amplitude, which is due to optical losses.

In Fig. 5, we present the color contour plot of the y -component of the magnetic field, H_y , and its distribution in the xz -plane for a TM-polarized electromagnetic field that propagates across the system with optimal thickness, $d = 100$ nm, at an incident angle $\alpha = 44.1^\circ$. The profile of the magnetic field component is clearly revealing an electromagnetic field that is localized at the chromium triiodide layer, with an evanescent nature in the insulating medium.

The symmetric bilayer structure. We also investigated the performance of a surface plasmon resonance in a symmetric bilayer structure, where a SiO₂ layer with thickness a is sandwiched between two identical layers CrI₃ of thickness $d=100$ nm (shown in Fig. 2b). We find that when light enters the system under the incident angle

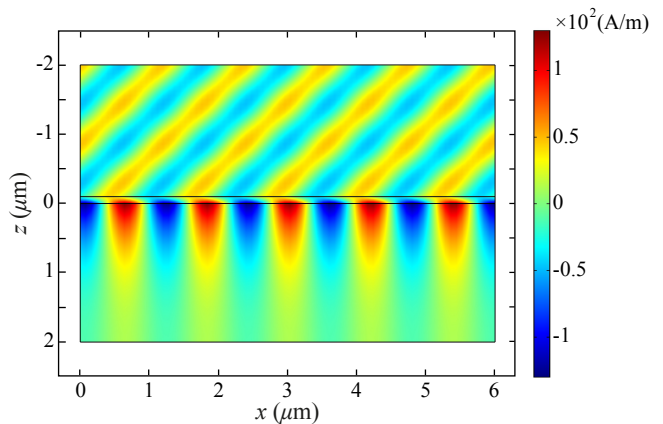


FIG. 5. Spatial distribution of magnetic field component H_y of TM polarized light through the system at the incident angle $\alpha = 44.1^\circ$, showing the propagation of surface electromagnetic waves bound by a CrI₃ layer with thickness $d = 100$ nm positioned at the $z = 0$ plane and its exponential decay in the insulating medium.

α the surface plasmons can be created on the interface between CrI₃ and air, and the position of the resonance angle increases in the range from 42.4° to 43.1° for a variation of spacer thickness (SiO₂ layer) between 450 and 520 nm. The results of the calculations are shown in Fig. 6. Note that for the excitation of surface plasmons at the outer boundary of the proposed system (i.e. at the CrI₃ layer interfaced between the glass prism and the SiO₂ layer), the electromagnetic wave should propagate through the spacer layer in the form of a guided mode that at the same time leads to the generation of an evanescent wave in the neighbouring low-refractive index medium. Therefore, it is clear that for plasmon generation, the spacer thickness a is optimal when it meets the value of any supported wave guide mode in the SiO₂ spacer layer. Meanwhile, when this condition is not fulfilled (for e.g. $a = 700$ nm, see violet dotted line in Fig. 6), the surface plasmon resonance vanishes from the spectrum.

Conclusion. In this paper, we addressed the properties of surface electromagnetic waves bound by a thin ferromagnet layer of chromium triiodide in the Kretschmann-Raether configuration. Using the conductivity tensor obtained within the Kubo formalism from the *ab initio* calculations, we evaluated the dispersion relation of surface plasmon polaritons. By a direct numerical solution to a set of Maxwell's equations we showed that in a rather large energy window these waves can be stabilized, and we have estimated the critical angle which corresponds to the absorption level of charge density waves in CrI₃. It turns out that this state inherits the properties of TM-surface plasmon polariton and its features are controlled by the thickness of CrI₃ layer, leading to the decrease in the effect with increasing layer thickness. We also examined the process of surface plasmon generation in the bilayer CrI₃ structures by considering the CrI₃/SiO₂/CrI₃

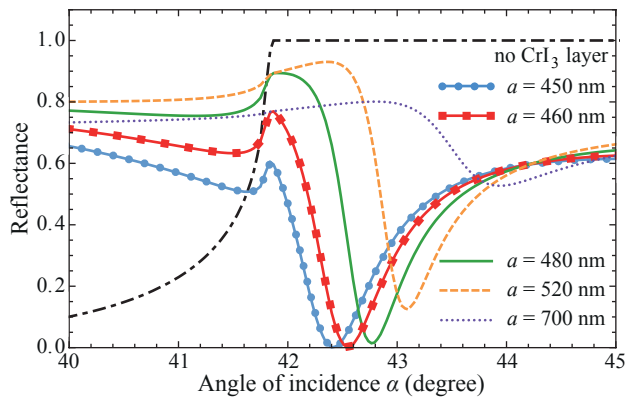


FIG. 6. Angular response of the system composed by two CrI_3 layers of thickness $d = 100$ nm separated by SiO_2 layer with thickness a and refractive index $n_{\text{SiO}_2} = 1.44$ (Fig. 2b). The light enters the system via the glass prism at the angle α . By varying the spacer thickness, the position of the reflectance minimum shifts from 42.4° at $a = 450$ nm (blue solid-circled line) to 43.1° at $a = 520$ nm (orange dashed line). All curves show a characteristic feature of total internal reflection as a local maximum at $\alpha = 41.8^\circ$. When the guided mode condition on the layer thickness is not fulfilled (e.g. when $a = 700$ nm) the surface plasmon resonance vanishes from the spectrum (violet, dotted line)

system when the light is injected to the system by a glass prism. We have shown that the angular position of the surface plasmon dip on the reflectance spectrum and its width strongly depend on the thickness of the SiO_2 layer. For surface plasmon generation the thickness of the spacer layer should support one of the guided modes. When the imposed condition is not fulfilled, the surface plasmons are not excited at the outer interface. It is the hope that the results of this theoretical analysis will trigger further experimental activity with new materials in the field of nanomagnetoplasmonics.

Acknowledgment. A.A.P. acknowledges support from the Russian Science Foundation Project No. 18-72-00058. The work of D.Y. was supported by the Swedish Research Council (Vetenskapsrådet, 2018-04383). V.K.G. and G.Y.G. acknowledge the support from the Ministry of Science and Technology and the National Center for Theoretical Sciences, Taiwan. O.E. and A.D. acknowledge support from the Knut and Alice Wallenberg foundation, the Swedish Research Council (Vetenskapsrådet), SERC and eSSSENCE. G.Y.G. thanks the support from the Academia Sinica Thematic Research Program (AS-106-TP-A07).

- [1] K. S. Novoselov, A. K. Geim, S. V. Morozov, D. Jiang, Y. Zhang, S. V. Dubonos, I. V. Grigorieva, and A. A. Firsov. Electric field effect in atomically thin carbon films. *Science*, 306(5696):666–669, 2004.
- [2] S. Manzeli, D. Ovchinnikov, D. Pasquier, O. V. Yazyev, and A. Kis. 2D transition metal dichalcogenides. *Nat. Rev. Mater.*, 2:17033, Jun 2017.
- [3] L. Li, Y. Yu, G. J. Ye, Q. Ge, X. Ou, H. Wu, D. Feng, X. H. Chen, and Y. Zhang. Black phosphorus field-effect transistors. *Nat. Nanotechnol.*, 9:372–377, Mar 2014.
- [4] H. Liu, A. T. Neal, Z. Zhu, Z. Luo, X. Xu, D. Tománek, and P. D. Ye. Phosphorene: An unexplored 2D semiconductor with a high hole mobility. *ACS Nano*, 8:4033–4041, Apr 2014.
- [5] P. Vogt, P. De Padova, C. Quaresima, J. Avila, E. Frantzeskakis, M. C. Asensio, A. Resta, B. Ealet, and G. Le Lay. Silicene: Compelling experimental evidence for graphenelike two-dimensional silicon. *Phys. Rev. Lett.*, 108:155501, Apr 2012.
- [6] B. Feng, Z. Ding, S. Meng, Y. Yao, X. He, P. Cheng, L. Chen, and K. Wu. Evidence of silicene in honeycomb structures of silicon on $\text{Ag}(111)$. *Nano Lett.*, 12:3507–3511, 2012.
- [7] A. Fleurence, R. Friedlein, T. Ozaki, H. Kawai, Y. Wang, and Y. Yamada-Takamura. Experimental evidence for epitaxial silicene on diboride thin films. *Phys. Rev. Lett.*, 108:245501, Jun 2012.
- [8] M. E. Dávila, L. Xian, S. Cahangirov, A. Rubio, and G. Le Lay. Germanene: a novel two-dimensional germanium allotrope akin to graphene and silicene. *New J. Phys.*, 16(9):095002, Sep 2014.
- [9] F.-F. Zhu, W.-J. Chen, Y. Xu, C.-L. Gao, D.-D. Guan, C.-H. Liu, D. Qian, S.-C. Zhang, and J.-F. Jia. Epitaxial growth of two-dimensional stanene. *Nat. Mater.*, 14:1020–1026, Aug 2015.
- [10] S. Lebégue, T. Björkman, M. Klintonberg, R. M. Nieminen, and O. Eriksson. Two-dimensional materials from data filtering and ab initio calculations. *Phys. Rev. X*, 3:031002, Jul 2013.
- [11] O. Eriksson. Searching for materials with reduced dimension. *Nat. Nanotechnol.*, 13(3):180, 2018.
- [12] N. Mounet et al. Two-dimensional materials from high-throughput computational exfoliation of experimentally known compounds. *Nat. Nanotechnol.*, 13(3):246, 2018.
- [13] F. B. Romdhane, O. Cretu, L. Debbichi, O. Eriksson, S. Lebégue, and F. Banhart. Quasi-2D Cu_2S crystals on graphene: In-situ growth and ab-initio calculations. *Small*, 11(11):1253–1257, 2015.
- [14] M.-W. Lin et al. Ultrathin nanosheets of CrSiTe_3 : a semiconducting two-dimensional ferromagnetic material. *J. Mater. Chem. C*, 4(2):315–322, 2016.
- [15] C. Gong, L. Li, Z. Li, H. Ji, A. Stern, Y. Xia, T. Cao, W. Bao, C. Wang, Y. Wang, Z. Q. Qiu, R. J. Cava, S. G. Louie, J. Xia, and X. Zhang. Discovery of intrinsic ferromagnetism in two-dimensional van der Waals crystals. *Nature*, 546:265–269, Apr 2017.
- [16] B. Huang et al. Layer-dependent ferromagnetism in a van der Waals crystal down to the monolayer limit. *Nature*, 546:270–273, Apr 2017.
- [17] D. Zhong, K. L. Seyler, X. Linpeng, R. Cheng, N. Sivadas, B. Huang, E. Schmidgall, T. Taniguchi, K. Watanabe, M. A. McGuire, W. Yao, D. Xiao, K.-

- M. C. Fu, and X. Xu. Van der Waals engineering of ferromagnetic semiconductor heterostructures for spin and valleytronics. *Sci. Adv.*, 3(5), 2017.
- [18] K. L. Seyler, D. Zhong, D. R. Klein, S. Gao, X. Zhang, B. Huang, E. Navarro-Moratalla, L. Yang, D. H. Cobden, M. A. McGuire, W. Yao, D. Xiao, P. Jarillo-Herrero, and X. Xu. Ligand-field helical luminescence in a 2D ferromagnetic insulator. *Nat. Phys.*, 14:277–281, Mar 2018.
- [19] S. Jiang, J. Shan, and K. F. Mak. Electric-field switching of two-dimensional van der Waals magnets. *Nat. Mater.*, 17:406–410, May 2018.
- [20] D. R. Klein et al. Probing magnetism in 2D van der Waals crystalline insulators via electron tunneling. *Science*, 360(6394):1218–1222, 2018.
- [21] Z. Wang et al. Electric-field switching of two-dimensional van der Waals magnets. *Nat. Commun.*, 9:2516, 2018.
- [22] B. Huang, G. Clark, D. R. Klein, D. MacNeill, E. Navarro-Moratalla, K. L. Seyler, N. Wilson, M. A. McGuire, D. H. Cobden, D. Xiao, W. Yao, P. Jarillo-Herrero, and X. Xu. Electrical control of 2d magnetism in bilayer CrI₃. *Nat. Nanotechnol.*, 13:544–548, Jul 2018.
- [23] N. D. Mermin and H. Wagner. Absence of ferromagnetism or antiferromagnetism in one- or two-dimensional isotropic Heisenberg models. *Phys. Rev. Lett.*, 17:1133–1136, Nov 1966.
- [24] W.-B. Zhang, Q. Qu, P. Zhu, and C.-H. Lam. Robust intrinsic ferromagnetism and half semiconductivity in stable two-dimensional single-layer chromium trihalides. *J. Mater. Chem. C*, 3:12457–12468, 2015.
- [25] J. L. Lado and J. Fernández-Rossier. On the origin of magnetic anisotropy in two dimensional CrI₃. *2D Mater.*, 4(3):035002, Jun 2017.
- [26] D. Torelli and T. Olsen. Calculating critical temperatures for ferromagnetic order in two-dimensional materials. *2D Mater.*, 6(1):015028, Dec 2018.
- [27] P. Jiang, L. Li, Z. Liao, Y. X. Zhao, and Z. Zhong. Spin direction-controlled electronic band structure in two-dimensional ferromagnetic CrI₃. *Nano Lett.*, 18:3844–3849, 2018.
- [28] Y. Fang, S. Wu, Z.-Z. Zhu, and G.-Y. Guo. Large magneto-optical effects and magnetic anisotropy energy in two-dimensional Cr₂Ge₂Te₆. *Phys. Rev. B*, 98:125416, Sep 2018.
- [29] C. Andersson et al. Influence of ligand states on the relationship between orbital moment and magnetocrystalline anisotropy. *Phys. Rev. Lett.*, 99:177207, Oct 2007.
- [30] J. M. Pitarke, V. M. Silkin, E. V. Chulkov, and P. M. Echenique. Theory of surface plasmons and surface-plasmon polaritons. *Rep. Prog. Phys.*, 70(1):1–87, Dec 2006.
- [31] J. A. Schuller, E. S. Barnard, W. Cai, Y. C. Jun, J. S. White, and M. L. Brongersma. Plasmonics for extreme light concentration and manipulation. *Nat. Mater.*, 9:193–204, Feb 2010.
- [32] J. A. Polo Jr. and A. Lakhtakia. Surface electromagnetic waves: A review. *Laser Photonics Rev.*, 5(2):234–246, 2011.
- [33] S. A. Mikhailov and K. Ziegler. New electromagnetic mode in graphene. *Phys. Rev. Lett.*, 99:016803, Jul 2007.
- [34] I. V. Iorsh, I. V. Shadrivov, P. A. Belov, and Y. S. Kivshar. Tunable hybrid surface waves supported by a graphene layer. *JETP Lett.*, 97:249–252, May 2013.
- [35] D. Yudin, O. Eriksson, and M. I. Katsnelson. Dynamics of quasiparticles in graphene under intense circularly polarized light. *Phys. Rev. B*, 91:075419, Feb 2015.
- [36] A. Kumar, A. Nemilentsau, K. Hung Fung, G. Hanson, N. X. Fang, and T. Low. Chiral plasmon in gapped Dirac systems. *Phys. Rev. B*, 93:041413, Jan 2016.
- [37] Z. Liu and K. Aydin. Localized surface plasmons in nanostructured monolayer black phosphorus. *Nano Lett.*, 16:3457–3462, Jun 2016.
- [38] D. Yudin, D. R. Gulevich, and I. A. Shelykh. Hybrid surface waves in two-dimensional Rashba-Dresselhaus materials. *Phys. Rev. B*, 95:035401, Jan 2017.
- [39] V. Kumar Gudelli and G.-Y. Guo. Magnetism and magneto-optical effects in bulk and few-layer CrI₃: a theoretical GGA+u study. *New J. Phys.*, 21(5):053012, May 2019.
- [40] G. Kresse and J. Furthmüller. Efficient iterative schemes for ab initio total-energy calculations using a plane-wave basis set. *Phys. Rev. B*, 54:11169–11186, Oct 1996.
- [41] G. Kresse and J. Furthmüller. Efficiency of ab-initio total energy calculations for metals and semiconductors using a plane-wave basis set. *Comput. Mat. Sci.*, 6(1):15–50, 1996.
- [42] J. P. Perdew, K. Burke, and M. Ernzerhof. Generalized gradient approximation made simple. *Phys. Rev. Lett.*, 77:3865–3868, Oct 1996.
- [43] H.-T. Jeng, G.-Y. Guo, and D. J. Huang. Charge-orbital ordering and Verwey transition in magnetite. *Phys. Rev. Lett.*, 93:156403, Oct 2004.
- [44] S. L. Dudarev, G. A. Botton, S. Y. Savrasov, C. J. Humphreys, and A. P. Sutton. Electron-energy-loss spectra and the structural stability of nickel oxide: An LSDA+U study. *Phys. Rev. B*, 57:1505–1509, Jan 1998.
- [45] B. Adolph, J. Furthmüller, and F. Bechstedt. Optical properties of semiconductors using projector-augmented waves. *Phys. Rev. B*, 63:125108, Mar 2001.
- [46] K. W. Chiu and J. J. Quinn. Plasma oscillations of a two-dimensional electron gas in a strong magnetic field. *Phys. Rev. B*, 9:4724–4732, Jun 1974.
- [47] E. Kretschmann and H. Raether. Radiative decay of non radiative surface plasmons excited by light. *Z. Naturforsch.*, 23A:2135–2136, Mar 1968.
- [48] A. V. Zayats, I. I. Smolyaninov, and Maradudin A. A. Nano-optics of surface plasmon polaritons. *Phys. Rep.*, 408(3):131–314, 2005.
- [49] S. K. Gray. Theory and modeling of plasmonic structures. *J. Phys. Chem. C*, 117(5):1983–1994, Feb 2013.
- [50] J. J. Foley IV, H. Harutyunyan, D. Rosenmann, R. Divan, G. P. Wiederrecht, and S. K. Gray. When are surface plasmon polaritons excited in the Kretschmann-Raether configuration? *Sci. Rep.*, 5:9929, Apr 2015.
- [51] Y. Akimov, M. E. Pam, and S. Sun. Kretschmann-Raether configuration: Revision of the theory of resonant interaction. *Phys. Rev. B*, 96:155433, Oct 2017.
- [52] A. P. Vinogradov, A. V. Dorofeenko, A. A. Pukhov, and A. A. Lisyansky. Exciting surface plasmon polaritons in the Kretschmann configuration by a light beam. *Phys. Rev. B*, 97:235407, Jun 2018.